https://dx.doi.org/10.1016/j.isatra.2023.09.013

Adaptive fixed-time sliding mode control for spacecraft reorientation with attitude pointing constraints and disturbance rejection

Tao Guan, Kai Zhang*, Bin Li

School of Aeronautics and Astronautics, Sichuan University, Chengdu, China

Xiaoyi Guan, Ka-Fai Cedric Yiu

Department of Applied Mathematics, The Hong Kong Polytechnic University, Hong Kong, China

Abstract

Spacecraft reorientation with attitude pointing constraints and the uncertainty of inertia and external disturbance is investigated in this paper. By introducing the potential function into the design of non-singular fixed-time sliding mode surface, the proposed controller can achieve fixed-time convergence and the convergence time of attitude error can be predetermined by selecting appropriate parameters. Meanwhile, the attitude pointing constraints can be satisfied all the time. The designed sliding surface and potential function have two equilibrium points, which guarantees the unwinding-free performance. Furthermore, an adaptive sliding mode control scheme is developed to handle the system lumped disturbance. Rigorous Lyapunov analyses are employed to ensure practical fixed-time closed-loop stability in the presence of system disturbance uncertainties and attitude pointing constraints. Therefore, the fixed-time stability, the feasibility of attitude pointing constraints and disturbance rejection are achieved simultaneously with the proposed controller. Numerical simulations are provided to demonstrate the effectiveness and superiority of the proposed method.

Keywords: Spacecraft Attitude Control, Fixed-time Stability, Sliding Mode

*Corresponding author

Control, Attitude Pointing Constraints, Adaptive Control.

1. Introduction

Spacecraft reorientation refers to the attitude maneuver of a spacecraft from the current value to a desired one. During attitude maneuver, spacecrafts carrying photosensitive sensors (such as telescopes) are not allowed to point directly towards the sun [1, 2]. Meanwhile, the communication antenna of the spacecraft is required to point towards the earth or a neighboring satellite for maintaining communications [1, 2, 3, 4]. Such restrictions are called attitude pointing constraints. In this article, the two types of attitude pointing constraints are addressed during the attitude maneuver.

Sliding mode control (SMC) [5, 6, 7, 8, 9, 10, 11, 12, 13] , an efficient nonlinear control scheme , has been widely researched in spacecraft attitude control, such as [14, 15, 16, 17]. In [18], a fast terminal sliding mode controller is proposed, and a finite-time convergence sliding mode controller is developed in [19]. Then, a fixed-time convergence sliding mode controller is proposed in [20]. Following these works, finite-time convergence sliding mode controller [21, 22] and fixed-time sliding mode controller [23, 24] are developed for the spacecraft attitude tracking. However, all of the SMC methods mentioned above can not deal with the attitude pointing constraints.

In most of the existing researches on tackling the attitude pointing constraints, there are mainly two streams. The first stream is called trajectory planning method, which utilizes geometric search algorithms or optimization methods for solving the attitude trajectory by considering attitude pointing constraints. For example, path search algorithm [3, 25] and optimal control method is utilized in [26, 27, 28] for calculating the maneuvering trajectory. Then, another controller has to be designed for tracking the planned attitude trajectory satisfying the attitude pointing constrains. The problem of this type of method is that the computation overhead is usually high. The second stream is based on the potential function (PF) method. The idea of this method is to

formulate the attitude pointing constraints into an energy-like functions, which is used for constructing the Lyapunov function in the controller design. A 'repulsive force' increases if the attitude gets closer to the surface of the attitude pointing constraint function, which forces the constraints to be satisfied. PF is usually integrated with other control schemes in order to obtain extra performance benefits. For example, there are PF-based proportional and derivative (PD) controller [29], PF-based backsteping controller [2], and PF-based sliding mode controller [30, 31]. However, only the asymptotic stability is obtained while the fixed-time convergence cannot be achieved in [2, 29, 30, 31]. To the best of our knowledge, the fixed-time convergence have not been achieved in the existing literature for handling the attitude pointing constrains.

The dynamics of rigid spacecraft is widely formulated by the quaternions as it can overcome singularity of Euler angles. Due to the redundancy of the unit quaternion definition, each attitude corresponds to two opposite quaternion, that is $(\boldsymbol{q}, -\boldsymbol{q})$. The "unwinding" phenomenon might occur, which may lead to unnecessarily large rotations of the spacecraft [29]. The unwinding phenomenon is solved by introducing the anti-unwinding potential function [2, 29, 31] and anti-unwinding sliding mode function [32, 16], but only asymptotic time stability is obtained. Recently, some fast convergence algorithms have been researched while considering unwinding-free performance, for example, the finite-time stability is achieved in [33, 34], and a fixed-time convergence controller is proposed in [35, 36]. However, in most of the existing literature, there are few anti-unwinding fixed-time convergence controllers for spacecraft reorientation task.

Robust adaptive stability has been achieved under both uncertainties and disturbances [37]. For further, robust adaptive finite-time convergence is obtained in [38]. The uncertainty of disturbance has been studied in the extensive literature on spacecraft attitude control. In [15, 16], the uncertainty has been overcome with the precisely known upper bound of disturbance. The adaptive control algorithms have been used to deal with the disturbance with unknown bound information in [17, 38, 22, 35], finite-time or fixed-time attitude convergence has been achieved, while considering uncertainty of inertia and external

disturbances. However, for spacecraft reorientation task, although the uncertainty of disturbance has been considered in [29, 30, 31], none of the preceding schemes have considered the fixed-time stability of spacecraft attitude control.

Motivated by these considerations, a novel PF-based non-singular fixed-time anti-unwinding sliding surface is proposed, which not only inherits the advantages of SMC, but also has the ability to deal with attitude pointing constraints. By applying the novel sliding surface and the adaptive control method, the practical fixed-time attitude convergence is achieved, while considering the attitude pointing constrains, the uncertainty of inertia and external disturbance torque, and the winding phenomenon. The main contributions are summarized as follows:

(1) By introducing the PF into the design of the non-singular fixed-time sliding surface, the fixed-time convergence and attitude pointing constrains can be satisfied simultaneously.

(2) An adaptive SMC scheme is proposed to achieve the disturbance rejection and ensure the fixed-time convergence of attitude error, although the upper bounds of the uncertainties of inertia matrix and external disturbances are unknown.

(3) By introducing the sign function into sliding surface and potential function, the unwinding phenomenon is also prevented.

The rest of this paper is organized as follows. Some preliminary results are given in Section 2. In Section 3, the adaptive fixed-time PF-based SMC law is proposed. In Section 4, some simulation results are given for testing the proposed method. Finally, some conclusions are made in Section 5.

2. Preliminaries

2.1. Notations, definitions and lemmas

Given the variable $\boldsymbol{x} = [x_1, x_2, \cdots, x_n]^\top \in \mathcal{R}^n$, the function $\text{sig}^\gamma(\boldsymbol{x})$ is defined by $\text{sig}^\gamma(\boldsymbol{x})=\left[|x_1|^\gamma \text{sign}(x_1), |x_2|^\gamma \text{sign}(x_2), \cdots, |x_n|^\gamma \text{sign}(x_n)\right]^\top$ with $\gamma > 0$, where $\text{sign}(\cdot)$ is the sign function. $\|\boldsymbol{x}\|_1$ and $\|\boldsymbol{x}\|$ represent the 1, 2 norms of

vector $\boldsymbol{x}$, respectively, satisfying that $\|\boldsymbol{x}\|_1 \geq \|\boldsymbol{x}\|$. $\boldsymbol{I}_n$ is an n dimensional identity matrix. For $\boldsymbol{y} = [y_1, y_2, y_3]^\top \in \mathcal{R}^3$, $\boldsymbol{y}^\times$ denotes the cross product of $\boldsymbol{y}$ and it is a skew-symmetric matrix given by $\boldsymbol{y}^\times = [0, -y_3, y_2; y_3, 0, -y_1; -y_2, y_1, 0]$.

The unit quaternion $\boldsymbol{q} = \left[q_0, \boldsymbol{q}_v^\top\right]^\top$ is used to describe spacecraft attitude, where $\boldsymbol{q}_v = [q_1, q_2, q_3]^\top$ is the vector part, q_0 is the scalar part and $\|\boldsymbol{q}\| = 1$. The identity quaternion $\boldsymbol{q}_I = [1, 0, 0, 0]^\top$ represents the origin in the attitude space. $(\cdot)^*$ is the quaternion conjugate and $\boldsymbol{q}^* = \left[q_0, -\boldsymbol{q}_v^\top\right]^\top$. For the quaternion $\boldsymbol{q}$ and $\boldsymbol{p}$, the quaternion multiplication $\otimes$ is defined as

$$\boldsymbol{q} \otimes \boldsymbol{p} = \begin{bmatrix} q_0 p_0 - \boldsymbol{q}_v^\top \boldsymbol{p}_v \\ q_0 \boldsymbol{p}_v + p_0 \boldsymbol{q} + \boldsymbol{q}_v^\times \boldsymbol{p}_v \end{bmatrix}$$

In addition, $\boldsymbol{q} \otimes \boldsymbol{p} = [\boldsymbol{q}]_L \boldsymbol{p}$ where $[\boldsymbol{q}]_L = q_0 \boldsymbol{I}_4 + \left[0, -\boldsymbol{q}_v^\top; \boldsymbol{q}_v, \boldsymbol{q}_v^\times\right]$.

Definition 1. *[20] Consider the following nonlinear system*

$$\dot{\boldsymbol{x}}(t) = \boldsymbol{f}(\boldsymbol{x}(t)),\ \boldsymbol{x}(0) = \boldsymbol{x}_0,\ \boldsymbol{f}(0) = 0,\ \boldsymbol{x}(t) \in \mathcal{R}^n \tag{1}$$

The origin of (1) is said to be globally finite-time stable if it is globally asymptotically stable and any solution $\boldsymbol{x}(t, \boldsymbol{x}_0)$ reaches the equilibrium point at some finite-time moment, i.e. $\boldsymbol{x}(t, \boldsymbol{x}_0) = 0, \forall t \geq T(\boldsymbol{x}_0)$, where $T : \mathcal{R}^n \to R_+ \cup \{0\}$ is a settling-time function. The origin of (1) is said to be fixed-time stable if it is globally finite-time stable and the settling-time function T is bounded, i.e., $\exists T_{\max} > 0 : T(\boldsymbol{x}_0) \leq T_{\max},\ \forall \boldsymbol{x}_0 \in \mathcal{R}^n$.

Lemma 1. *[1] Consider system (1), if there exists a continuous radially unbounded function $V : \mathcal{R}^n \to R_+ \cup \{0\},\ V(0) = 0$ such that*

$$\dot{V}(\boldsymbol{x}(t)) \leq -\left(p_1 V^{\rho_1}(\boldsymbol{x}(t)) + p_2 V^{\rho_2}(\boldsymbol{x}(t))\right)^v + \vartheta$$

where $0 < \vartheta < \infty$, p_1, p_2, ρ_1, ρ_2 and v are positive constants with $\rho_1 v < 1$ and $\rho_2 v > 1$. Then, the system is practical fixed-time stable. Moreover, the trajectories of the closed-loop system is bounded in fixed time T as

$$\left\{ \lim_{t \to T} \boldsymbol{x}(t) \mid V(\boldsymbol{x}(t)) \leq \min \left\{ p_1^{-\frac{1}{\rho_1}} \left(\frac{\vartheta}{1-\theta^v} \right)^{\frac{1}{v\rho_1}}, p_2^{-\frac{1}{\rho_2}} \left(\frac{\vartheta}{1-\theta^v} \right)^{\frac{1}{v\rho_2}} \right\} \right\}$$

where $0 < \theta \leq 1$ is a scalar and the fixed-time T is bounded by

$$T \leq 1/\left(p_1^v \theta^v \left(1-\rho_1 v\right)\right) + 1/\left(p_2^v \theta^v \left(\rho_2 v - 1\right)\right)$$

Lemma 2. *[39] Given variable $x, y \in \mathcal{R}$, and $p > 1$, $q > 1$ such that $(p-1)(q-1) = 1$, $\forall \epsilon > 0$, the inequality $xy \leq \frac{\epsilon^p}{p}|x|^p + \frac{1}{q\epsilon^q}|y|^q$ holds.*

Lemma 3. *[40] Given variable $\boldsymbol{x} = [x_1, x_2, \cdots, x_n] \in \mathcal{R}^n$, the inequality $\sum_{i=1}^n |x_i|^{1+p} \geqslant \left(\sum_{i=1}^n |x_i|^2\right)^{(1+p)/2}$ holds, where $p \in (0,1)$ is a real number.*

Lemma 4. *[41] Given variable $\boldsymbol{x} = [x_1, x_2, \cdots, x_n] \in \mathcal{R}^n$, the inequality $\sum_{i=1}^n |x_i|^p \geqslant n^{1-p}\left(\sum_{i=1}^n |x_i|\right)^p$ holds, where $p > 1$ is a real number.*

2.2. Attitude error kinematics and dynamics of rigid spacecraft

According to [17], the quaternion-based attitude error kinematics and dynamics of a rigid spacecraft can be described by

$$\begin{cases} \boldsymbol{J}\dot{\boldsymbol{\omega}}_e + \boldsymbol{J}\left(\boldsymbol{G}\dot{\boldsymbol{\omega}}_d - \boldsymbol{\omega}_e^{\times}\boldsymbol{G}\boldsymbol{\omega}_d\right) + \boldsymbol{\omega}^{\times}\boldsymbol{J}\boldsymbol{\omega} = \boldsymbol{u} + \boldsymbol{d} \\ \dot{\boldsymbol{q}}_{ev} = \frac{1}{2}\left(q_{e0}\boldsymbol{\omega}_e + \boldsymbol{q}_{ev}^{\times}\boldsymbol{\omega}_e\right) \\ \dot{q}_{e0} = -\frac{1}{2}\boldsymbol{q}_{ev}^T\boldsymbol{\omega}_e,\ \boldsymbol{\omega}_e = \boldsymbol{\omega} - \boldsymbol{G}\boldsymbol{\omega}_d \end{cases} \tag{2}$$

where $\boldsymbol{q}_e = [q_{e0},\ \boldsymbol{q}_{ev}^{\top}]^{\top}$ is the unit error quaternion which can be given by $\boldsymbol{q}_e = \boldsymbol{q}_d^* \otimes \boldsymbol{q}$, $q_{e0} \in \mathcal{R}$, $\boldsymbol{q}_{ev} \in \mathcal{R}^3$, $\|\boldsymbol{q}_e\| = 1$, $\boldsymbol{\omega} \in \mathcal{R}^3$ and $\boldsymbol{\omega}_e \in \mathcal{R}^3$ represent angular velocity and angular velocity error with respect to inertial frame, respectively, $G\left(\boldsymbol{q}_e\right) = \left(q_{e0}^2 - \boldsymbol{q}_{ev}^{\top}\boldsymbol{q}_v\right)\boldsymbol{I}_3 + 2\boldsymbol{q}_{ev}\boldsymbol{q}_{ev}^{\top} - 2q_{e0}\boldsymbol{q}_{ev}^{\times}$ is the rotation matrix, $\boldsymbol{\omega}_d \in \mathcal{R}^3$ is the desired angular velocity, $\boldsymbol{u} = [u_1, u_2, u_3] \in \mathcal{R}^3$ stands for the control torque, $\boldsymbol{J} = \boldsymbol{J}_0 + \Delta\boldsymbol{J} \in \mathcal{R}^{3\times 3}$ denotes the symmetric and positive definite inertia matrix, $\boldsymbol{J}_0$ is the nominal value of the inertia matrix $\boldsymbol{J}$, $\Delta\boldsymbol{J}$ is the inertia uncertainty, and $\boldsymbol{d} \in \mathcal{R}^3$ is the external disturbance torques.

A rest-to-rest attitude maneuver is considered in this paper, it follows that $\boldsymbol{\omega}_d = \dot{\boldsymbol{\omega}}_d = \boldsymbol{0}$. According to (2), one has $\boldsymbol{\omega}_e = \boldsymbol{\omega}$. Then, the unit-quaternion error kinematics and dynamics of rigid spacecraft can be written as

$$\dot{\boldsymbol{q}}_e = \frac{1}{2}\boldsymbol{q}_e \otimes \tilde{\boldsymbol{\omega}} = \frac{1}{2}\begin{bmatrix} -\boldsymbol{q}_{ev}^{\top} \\ \boldsymbol{q}_{ev}^{\times} + q_{e0}\boldsymbol{I}_3 \end{bmatrix}\boldsymbol{\omega} \tag{3}$$

$$\boldsymbol{J}\dot{\boldsymbol{\omega}} = -\boldsymbol{\omega}^{\times}\boldsymbol{J}\boldsymbol{\omega} + \boldsymbol{u}_t + \boldsymbol{d} \tag{4}$$

where $\tilde{\boldsymbol{\omega}} = [0, \boldsymbol{\omega}]$.

For dynamics of rigid spacecraft in (4), we make the following assumptions.

Assumption 1. *For symmetric positive-definite inertia matrix $\boldsymbol{J}$, the following properties are assumed to be satisfied*

$$\|\boldsymbol{J}\| \leq \Im, \|\dot{\boldsymbol{J}}\| \leq \bar{\Im} \tag{5}$$

$$\lambda_{\min}(\boldsymbol{J}) \|\boldsymbol{x}\|^2 \leq \boldsymbol{x}^{\top}\boldsymbol{J}\boldsymbol{x} \leq \lambda_{\max}(\boldsymbol{J}) \|\boldsymbol{x}\|^2, \forall \boldsymbol{x} \in \mathcal{R}^3 \tag{6}$$

where $\Im$ and $\bar{\Im}$ are unknown positive constants, $\lambda_{\min}(\boldsymbol{J})$ and $\lambda_{\max}(\boldsymbol{J})$ are minimum and maximum eigenvalue of $\boldsymbol{J}$, respectively.

Assumption 2. *The external disturbance $\boldsymbol{d}$ is assumed to satisfy $\|\boldsymbol{d}\| \leq \bar{d}$, where $\bar{d}$ is an unknown positive constant.*

2.3. Attitude pointing constraints

As illustrated in Fig. 1, during the attitude maneuver, the attitude not only is required to move from the current value to the desired one, but also has to be kept outside of a forbidden zone while inside of a mandatory zone [2].

Attitude Forbidden Zone is defined by a set of attitudes that prevent the optical sensor of the spacecraft from direct exposure to certain celestial objects. For example, the sun and the moon. As shown in Fig. 1, $\boldsymbol{x}_{1j}$, $j = 1, 2, \cdots, n$, denotes the jth object vector, which is a unit vector pointing towards the jth unwanted object in the inertial frame. Let $\boldsymbol{y}_1$ and $\boldsymbol{y}_1^{'}$ be the unit sensor boresight vector in the body frame and the inertial frame, respectively. Then, it follows that

$$\boldsymbol{y}_1^{'} = \boldsymbol{R}^{\top}(\boldsymbol{q})\,\boldsymbol{y}_1 \tag{7}$$

where $\boldsymbol{R}(\boldsymbol{q}) = \left(q_0^2 - \boldsymbol{q}_v^{\top}\boldsymbol{q}_v\right)\boldsymbol{I}_3 + 2\boldsymbol{q}_v\boldsymbol{q}_v^{\top} - 2q_0\boldsymbol{q}_v^{\times}$ is the rotation matrix. Thus, the attitude forbidden zone can be expressed by the following attitude constraint:

$$\boldsymbol{x}_{1j}^{\top}\boldsymbol{y}_1^{'} > \cos\theta_{jmin} \tag{8}$$

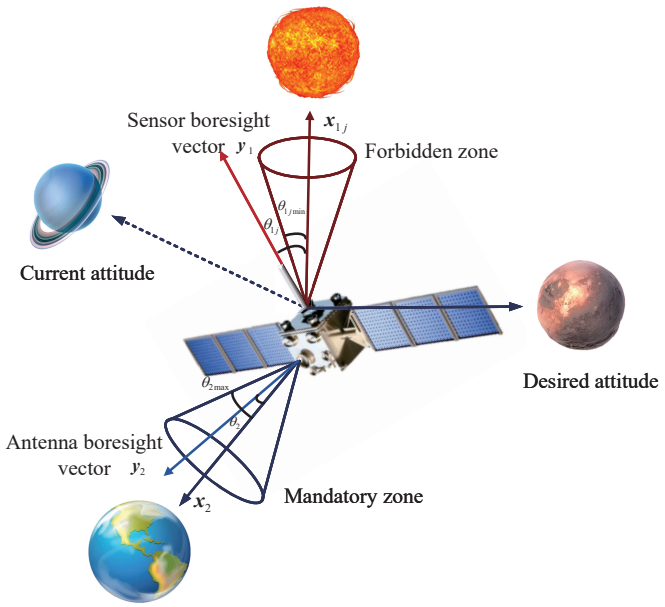

Fig. 1. Attitude constrained spacecraft reorientation.

Attitude Mandatory Zone is defined by a set of attitudes that ensure the communication antenna pointing towards a ground base station or a neighboring satellite. As illustrated in Fig. 1, $\boldsymbol{x}_2$ represents a unit vector pointing to a ground base station in the inertial frame. $\boldsymbol{y}_2$ and $\boldsymbol{y}_2^{'}$ denote the unit antenna vector in the body frame and the inertial frame, respectively, and $\boldsymbol{y}_2^{'}$ can be obtained by $\boldsymbol{y}_2^{'} = \boldsymbol{R}^{\top}(\boldsymbol{q})\,\boldsymbol{y}_2$. The attitude mandatory zone can be expressed by the following attitude constraint:

$$\boldsymbol{x}_2^{\top}\boldsymbol{y}_2^{'} < \cos\theta_{2max} \tag{9}$$

According to [2], (8) and (9) can be rewritten into the following convex form:

$$\boldsymbol{q}^{\top}\boldsymbol{M}_{1j}\boldsymbol{q} < 0,\ \boldsymbol{q}^{\top}\boldsymbol{M}_{2}\boldsymbol{q} > 0 \tag{10}$$

where

$$\boldsymbol{M}_{1j} = \begin{bmatrix} \boldsymbol{x}_{1j}^{\top}\boldsymbol{y}_1 & \boldsymbol{y}_1^{\times}\boldsymbol{x}_{1j}{}^{\top} \\ \boldsymbol{y}_1^{\times}\boldsymbol{x}_{1j} & A_{1j} \end{bmatrix} - \cos\theta_{jmin}\boldsymbol{I}_4 \tag{11}$$

$A_{1j} = \boldsymbol{x}_{1j}\boldsymbol{y}_1^T + \boldsymbol{y}_1\boldsymbol{x}_{1j}^\top - \boldsymbol{x}_{1j}^\top\boldsymbol{y}_1$, and $\boldsymbol{M}_2$ is similarly defined as $\boldsymbol{M}_{1j}$. Noting that $\boldsymbol{q}_d^* \otimes \boldsymbol{q}_d = \boldsymbol{q}_I$, the convex form of (10) can be rewritten as

$$\boldsymbol{q}_e^\top \tilde{\boldsymbol{M}}_{1j}\boldsymbol{q}_e < 0,\ \boldsymbol{q}_e^\top \tilde{\boldsymbol{M}}_2\boldsymbol{q}_e > 0$$

where $\tilde{\boldsymbol{M}}_{1j} = \left([\boldsymbol{q}_d]_L\right)^\top \boldsymbol{M}_{1j}\,[\boldsymbol{q}_d]_L$ and $\tilde{\boldsymbol{M}}_2$ can be obtained in a similar manner.

3. Adaptive fixed-time disturbance rejection controller design

In this section, a novel fixed-time PF-based sliding surface is proposed to address attitude pointing constrains. Then an adaptive SMC scheme and update strategy of parameters are presented for handling the inertial uncertainty and external disturbance torque.

3.1. Potential function

Following [42], a modified version is constructed as below:

$$V_p = V_a + V_a \underbrace{\left\{ \sum_{j=1}^{n} \varrho_{1j} e^{(\delta\varphi_{1j})^{-1}} + \varrho_2 e^{(\delta\varphi_2)^{-1}} \right\}}_{V_r} \tag{12}$$

where $V_a(\boldsymbol{q}_e) = \|\boldsymbol{q}_e - \mathrm{sign}\,(q_{e0})\,\boldsymbol{q}_I\|^2$ is the attractive potential function, V_r is the repulsive potential function, $\varphi_{1j} = -\boldsymbol{q}_e{}^\top \tilde{\boldsymbol{M}}_{1j}\boldsymbol{q}_e > 0$, $\varphi_2 = \boldsymbol{q}_e^\top \tilde{\boldsymbol{M}}_2\boldsymbol{q}_e > 0$, ϱ_{1j} and ϱ_2 are positive weighting parameters, and $\delta > 0$ is a design variable.

Lemma 5. *The potential function (12) has the following properties:*
1) $V_p(\boldsymbol{q}_e) \geq 0$, $\forall \boldsymbol{q}_e$ and $V_p = 0$ if and only if $\boldsymbol{q}_e = \pm\boldsymbol{q}_I$;
2) $V_r > \varrho$, where $\varrho = \min\{\varrho_{1j}, \varrho_2\} > 0$, $j = 1, 2, \ldots, n$.

For obtaining more potential function information, the gradient of V_p is given by

$$\nabla V_p = \nabla V_a (V_r + 1) + V_a \nabla V_r \tag{13}$$

where

$$\nabla V_r = \sum_{j=1}^{n} \frac{2\delta\varrho_{1j}}{(\delta\varphi_{1j})^2} e^{(\delta\varphi_{1j})^{-1}} \tilde{\boldsymbol{M}}_{1j}\boldsymbol{q}_e + \frac{-2\delta\varrho_2}{(\delta\varphi_2)^2} e^{(\delta\varphi_2)^{-1}} \tilde{\boldsymbol{M}}_2\boldsymbol{q}_e$$

The Hessian matrix of V_p can be derived as

$$\nabla^2 V_p = \nabla^2 V_a \left(V_r + 1\right) + 2\nabla V_a \nabla V_r^\top + V_a \nabla^2 V_r \tag{14}$$

where

$$\begin{aligned}
\nabla^2 V_r = & \sum_{j=1}^{n} \frac{2\delta \varrho_{1j} e^{(\delta\varphi_{1j})^{-1}}}{\left(\delta\varphi_{1j}\right)^4} \\
& \left(\left(\delta\varphi_{1j}\right)^2 \tilde{\boldsymbol{M}}_{1j} + 4\delta \left(\delta\varphi_{1j}\right) \tilde{\boldsymbol{M}}_{1j} \boldsymbol{q}_e \boldsymbol{q}_e^\top \tilde{\boldsymbol{M}}_{1j} + 2\delta \tilde{\boldsymbol{M}}_{1j} \boldsymbol{q}_e \boldsymbol{q}_e{}^\top \tilde{\boldsymbol{M}}_{1j} \right) \\
& - \frac{2\delta \varrho_2 e^{(\delta\varphi_2)^{-1}}}{\left(\delta\varphi_2\right)^4} \left(\left(\delta\varphi_2\right)^2 \tilde{\boldsymbol{M}}_2 - 4\delta \left(\delta\varphi_2\right) \tilde{\boldsymbol{M}}_2 \boldsymbol{q}_e \boldsymbol{q}_e^\top \tilde{\boldsymbol{M}}_2 - 2\delta \tilde{\boldsymbol{M}}_2 \boldsymbol{q}_e \boldsymbol{q}_e^\top \tilde{\boldsymbol{M}}_2 \right)
\end{aligned} \tag{15}$$

3.2. A PF-based SMC

A novel PF-based fixed-time anti-unwinding sliding surface is constructed as follows:

$$\boldsymbol{S} = (\boldsymbol{\omega} - \mu\hat{\boldsymbol{\omega}}) V_r + \operatorname{sign}\left(q_{e0}\right) \boldsymbol{f}(\boldsymbol{q}_{ev}) \tag{16}$$

where $\hat{\boldsymbol{\omega}} = -\operatorname{Vec}\left(\boldsymbol{q}_e{}^* \otimes \nabla V_p\right)$, $\operatorname{Vec}\left(\boldsymbol{q}\right)$ denotes the vector part of $\boldsymbol{q}$, $\boldsymbol{f}(\boldsymbol{q}_{ev}) = [f_1(q_{e1}), f_2(q_{e2}), f_3(q_{e3})]^\top$,

$$f_i(q_{ei}) = \begin{cases} k_{21}\mathrm{sig}^{\alpha_2}(q_{ei}) + k_{22}\mathrm{sig}^{\beta_2}(q_{ei}), & \text{if } |q_{ei}| \geq \varepsilon \\ l_1 q_{ei} + l_2 \mathrm{sign}(q_{ei}) q_{ei}^2, & \text{if } |q_{ei}| < \varepsilon \end{cases} \tag{17}$$

the switching method (17) is used to avoid the singularity, $\varepsilon > 0$ is a small constant, μ, k_{21}, $k_{22} > 0$ are the positive constants, $0 < \alpha_2 < 1$, $\beta_2 > 1$, $l_1 = k_{21}\left(2 - \alpha_2\right)\varepsilon^{\alpha_2 - 1} + k_{22}\left(2 - \beta_2\right)\varepsilon^{\beta_2 - 1}$ and $l_2 = k_{21}\left(\alpha_2 - 1\right)\varepsilon^{\alpha_2 - 2} + k_{22}\left(\beta_2 - 1\right)\varepsilon^{\beta_2 - 2}$ are deigned to ensure the existence of $\dot{f}_i(q_{ei})$ around $|q_{ei}| = \varepsilon$.

Remark 1. By introducing the term $\hat{\boldsymbol{\omega}} = -\operatorname{Vec}\left(\boldsymbol{q}_e{}^* \otimes \nabla V_p\right)$ into the sliding function (16), the constructed sliding surface $\boldsymbol{S}$ not only has the ability of handling the attitude pointing constraints, but also can guarantee the practical fixed-time convergence, which will be shown in Theorem 1.

3.3. Controller Design

Then, an adaptive SMC control law is designed below

$$\boldsymbol{u} = \left(-\boldsymbol{K}_{11}\mathrm{sig}^{\alpha_1}(\boldsymbol{S}) - \boldsymbol{K}_{12}\mathrm{sig}^{\beta_1}(\boldsymbol{S})\right)/V_r + \boldsymbol{u}_{ad} \tag{18}$$

where $0 < \alpha_1 < 1$, $\beta_1 > 1$, $\mu > 0$, $\boldsymbol{K}_{11} = k_{11}\boldsymbol{I}_3$, $\boldsymbol{K}_{12} = k_{12}\boldsymbol{I}_3$,

$$\dot{f}_i(q_{ei}) = \begin{cases} (k_{21}\alpha_2|q_{ei}|^{\alpha_2-1} + k_{22}\beta_2|q_{ei}|^{\beta_2-1})\dot{q}_{ei}, & \text{if } |q_{ei}| \geq \varepsilon \\ (l_1 + 2l_2\,|q_{ei}|)\,\dot{q}_{ei}, & \text{if } |q_{ei}| < \varepsilon \end{cases}$$

and

$$\begin{aligned} \dot{\hat{\boldsymbol{\omega}}} &= \frac{\mathrm{d}\hat{\boldsymbol{\omega}}}{\mathrm{d}t} = -\frac{\mathrm{d}\left(\mathrm{Vec}\left(\boldsymbol{q}_e{}^* \otimes \nabla V_p\right)\right)}{\mathrm{d}t} \\ &= -\mathrm{Vec}\left(\dot{\boldsymbol{q}}_e^* \otimes \nabla V_p + \boldsymbol{q}_e{}^* \otimes \left[\nabla^2 V_p \dot{\boldsymbol{q}}_e\right]\right) \\ &= -\mathrm{Vec}\left(\left(\frac{1}{2}\boldsymbol{q}_e \otimes \tilde{\boldsymbol{\omega}}\right)^* \otimes \nabla V_p + \boldsymbol{q}_e{}^* \otimes \left[\nabla^2 V_p(\frac{1}{2}\boldsymbol{q}_e \otimes \tilde{\boldsymbol{\omega}})\right]\right) \end{aligned}$$

The part of adaptive compensation $\boldsymbol{u}_{ad}$ is given by

$$\boldsymbol{u}_{ad} = -\hat{\gamma}\eth V_r^{-1}\boldsymbol{S} \tag{19}$$

where $\eth = V_r^2\|\boldsymbol{\omega}\|^4 + V_r^2 + \left(\mu V_r\|\dot{\hat{\boldsymbol{\omega}}}\| + \|\dot{V}_r\|\|(\boldsymbol{\omega} - \mu\hat{\boldsymbol{\omega}})\| + \|\dot{\boldsymbol{f}}(\boldsymbol{q}_{ev})\|\right)^2 + 1$, $\dot{V}_r = \frac{1}{2}\left(\nabla V_r\right)^\top \begin{bmatrix} -\boldsymbol{q}_{ev}^\top \\ \boldsymbol{q}_{ev}^\times + q_{e0}\boldsymbol{I}_3 \end{bmatrix} \boldsymbol{\omega}$, $\hat{\gamma}$ represents the estimation value of γ, γ is an unknown positive constant which will be stated later, and the corresponding adaptive update law is designed as

$$\dot{\hat{\gamma}} = \sigma\left(-\varsigma\hat{\gamma} + \eth\|\boldsymbol{S}\|^2\right) \tag{20}$$

where $\sigma, \varsigma > 0$.

By applying the proposed control law (18) to system (3) and (4), the practical fixed-time convergence, the satisfaction of attitude pointing constraints (8) and (9) and disturbance rejection capability are proven by the following theorem.

Theorem 1. *Applying control law* (18) *to system* (3) *and* (4)*, the following statements can be verified.*

(*i*) $\boldsymbol{S}$ *and* $\hat{\gamma}$ *are uniformly ultimately bounded.*

(*ii*) V_r *is bounded, and the attitude pointing constraints* (8) *and* (9) *are satisfied all the time.*

(*iii*)

$$\lim_{t\to T_1}\|\boldsymbol{S}\|\leq S_m$$

where S_m *is a positive constant and* T_1 *is bounded by* $T_1\leq 1/\left(\kappa_{11}\theta\left(\lambda_{11}-1\right)\right)+1/\left(\kappa_{12}\theta\left(1-\lambda_{12}\right)\right)$, $\lambda_{11}=\frac{1}{2}\left(\alpha_1+1\right)>1$, $0<\lambda_{12}=\frac{1}{2}\left(\beta_1+1\right)<1$, $\kappa_{11}=2^{\lambda_{11}}3^{1-\lambda_{11}}\lambda_{min}\left(\boldsymbol{K}_{11}\right)$, $\kappa_{12}=2^{\lambda_{12}}\lambda_{min}\left(\boldsymbol{K}_{12}\right)$, *and* θ *is a scalar satisfying* $0<\theta\leq 1$.

(*iv*) *After the attitude trajectory reaches the sliding surface, the attitude error quaternion* $\boldsymbol{q}_e$ *would converge to a small neighborhood of the desired value* $\pm\boldsymbol{q}_I$ *and angular velocity* $\boldsymbol{\omega}$ *would converge to a small neighborhood of zero in a fixed-time* T_3, *i.e.,*

$$\begin{aligned}&\lim_{t\to T_3}|q_{ei}|\leq\varepsilon_q,\ \lim_{t\to T_3}|\omega_i|\leq\varepsilon_\omega\\&\varepsilon_q:=\max\{\varepsilon_{ev},\varepsilon\},\ \varepsilon_\omega:=\mu\varepsilon_{\hat{\omega}}+\left(\varepsilon_f+S_m\right)/\varrho\end{aligned}\tag{21}$$

where $\varepsilon_f:=k_{21}\varepsilon_q^{\alpha_2}+k_{22}\varepsilon_q^{\beta_2}$, $T_3=T_1+T_2$, T_2 *is bounded by* $T_2\leq 1/\left(\kappa_{22}\theta_1\left(1-\lambda_{22}\right)\right)+1/\left(\kappa_{21}\theta_1\left(\lambda_{21}-1\right)\right)$, $\lambda_{21}=\frac{1}{2}\left(\alpha_2+1\right)>1$, $0<\lambda_{22}=\frac{1}{2}\left(\beta_2+1\right)<1$, $\kappa_{21}=\frac{k_{21}}{2V_{r,\max}}3^{1-\lambda_{21}}$ *and* $\kappa_{22}=\frac{k_{22}}{2V_{r,\max}}$, $V_{r,\max}$ *is maximum value of* V_r.

Proof (*i*) Construct a Lyapunov function as follows:

$$V_1=\frac{1}{2}\boldsymbol{S}^\top\boldsymbol{J}\boldsymbol{S}+\frac{1}{2\sigma}\tilde{\gamma}^2\tag{22}$$

where $\tilde{\gamma}=\gamma-\hat{\gamma}$. In view of system (3) and (4), the derivative of V_1 with respect to t can be given as

$$\begin{aligned}\dot{V}_1&=\boldsymbol{S}^\top\boldsymbol{J}\dot{\boldsymbol{S}}+\frac{1}{2}\boldsymbol{S}^\top\dot{\boldsymbol{J}}\boldsymbol{S}+\frac{1}{\sigma}\tilde{\gamma}\dot{\tilde{\gamma}}\\&=\boldsymbol{S}^\top\Bigg(V_r\Big(-\boldsymbol{\omega}^\times\boldsymbol{J}\boldsymbol{\omega}+\boldsymbol{u}+\boldsymbol{d}-\mu\boldsymbol{J}\dot{\hat{\boldsymbol{\omega}}}\Big)+\dot{V}_r\boldsymbol{J}(\boldsymbol{\omega}-\mu\hat{\boldsymbol{\omega}})\\&+\operatorname{sign}\left(q_{e0}\right)\boldsymbol{J}\dot{\boldsymbol{f}}(\boldsymbol{q}_{ev})\Bigg)+\frac{1}{2}\boldsymbol{S}^\top\dot{\boldsymbol{J}}\boldsymbol{S}-\tilde{\gamma}\dot{\hat{\gamma}}/\sigma\end{aligned}\tag{23}$$

By applying Assumption 1, Assumption 2 and Young's inequality in Lemma 2, it follows that

$$
\begin{aligned}
-V_r\boldsymbol{S}^\top\boldsymbol{\omega}^\times\boldsymbol{J}\boldsymbol{\omega} &\le V_r\|\boldsymbol{J}\|\|\boldsymbol{\omega}\|^2\|\boldsymbol{S}\| \le \Im V_r\|\boldsymbol{\omega}\|^2\|\boldsymbol{S}\| \\
&\le \chi\Im V_r^2\|\boldsymbol{\omega}\|^4\|\boldsymbol{S}\|^2 + \frac{\Im}{4\chi} \qquad (24)\\
V_r\boldsymbol{S}^\top\boldsymbol{d} &\le \chi\bar{d}V_r^2\|\boldsymbol{S}\|^2 + \frac{\bar{d}}{4\chi} \qquad (25)\\
\boldsymbol{S}^\top&\Big(-\mu V_r\boldsymbol{J}\dot{\hat{\boldsymbol{\omega}}} + \dot{V}_r\boldsymbol{J}(\boldsymbol{\omega}-\mu\hat{\boldsymbol{\omega}}) + \operatorname{sign}(q_{e0})\,\boldsymbol{J}\dot{\boldsymbol{f}}(\boldsymbol{q}_{ev})\Big) \\
&\le \chi\Im\|\boldsymbol{S}\|^2\left(\mu V_r\|\dot{\hat{\boldsymbol{\omega}}}\| + \|\dot{V}_r\|\|(\boldsymbol{\omega}-\mu\hat{\boldsymbol{\omega}})\| + \|\dot{\boldsymbol{f}}(\boldsymbol{q}_{ev})\|\right)^2 + \frac{\Im}{4\chi} \qquad (26)\\
\frac{1}{2}&\boldsymbol{S}^\top\dot{\boldsymbol{J}}\boldsymbol{S} \le \frac{1}{2}\bar{\Im}\|\boldsymbol{S}\|^2 \qquad (27)
\end{aligned}
$$

Then, combining (23), (24), (25),(26) and (27) yields

$$
\begin{aligned}
\dot{V}_1 \le& V_r\boldsymbol{S}^\top\boldsymbol{u} + \Big(\chi\Im V_r^2\|\boldsymbol{\omega}\|^4 + \chi\bar{d}V_r^2 + \chi\Im\Big(\mu V_r\|\dot{\hat{\boldsymbol{\omega}}}\| + \|\dot{V}_r\|\|(\boldsymbol{\omega}-\mu\hat{\boldsymbol{\omega}})\| \\
&+ \|\dot{\boldsymbol{f}}(\boldsymbol{q}_{ev})\|\Big)^2 + \frac{1}{2}\bar{\Im}\Big)\|\boldsymbol{S}\|^2 - \tilde{\gamma}\dot{\hat{\gamma}}/\sigma + \frac{\bar{d}}{4\chi} + \frac{\Im}{2\chi} \\
\le& V_r\boldsymbol{S}^\top\boldsymbol{u} + \gamma\eth\|\boldsymbol{S}\|^2 - \tilde{\gamma}\dot{\hat{\gamma}}/\sigma + \frac{\bar{d}}{4\chi} + \frac{\Im}{2\chi} \qquad (28)
\end{aligned}
$$

where $\gamma = \max\left\{\chi\Im, \chi\bar{d}, \frac{1}{2}\bar{\Im}\right\}$ is the the unknown positive constant, and $\eth$ is defined in (19).

Considering adaptive update law (20) and the Young's inequality in Lemma 2, one has

$$
\begin{aligned}
-\tilde{\gamma}\dot{\hat{\gamma}}/\sigma &= -\tilde{\gamma}\eth\|\boldsymbol{S}\|^2 + \varsigma\tilde{\gamma}\hat{\gamma} \qquad (29)\\
\varsigma\tilde{\gamma}\hat{\gamma} &= \varsigma\tilde{\gamma}\left(-\tilde{\gamma}+\gamma\right) \le -\frac{\varsigma}{2}\tilde{\gamma}^2 + \frac{\varsigma}{2}\gamma^2 \qquad (30)
\end{aligned}
$$

Substituting (29),(30) and the designed control law (18) into (28) yields

$$
\begin{aligned}
\dot{V}_1 \le& \boldsymbol{S}^\top\Big(-\boldsymbol{K}_{21}\mathrm{sig}^{\alpha_1}(\boldsymbol{S}) - \boldsymbol{K}_{22}\mathrm{sig}^{\beta_1}(\boldsymbol{S}) \\
&- \hat{\gamma}\eth\boldsymbol{S}\Big) + \gamma\eth\|\boldsymbol{S}\|^2 - \tilde{\gamma}\eth\|\boldsymbol{S}\|^2 - \frac{\varsigma}{2}\tilde{\gamma}^2 + \frac{\varsigma}{2}\gamma^2 + \frac{\bar{d}}{4\chi} + \frac{\Im}{2\chi} \\
\le& -\kappa_{11}\left(\frac{1}{2}\boldsymbol{S}^\top\boldsymbol{J}\boldsymbol{S}\right)^{\lambda_{11}} - \kappa_{12}\left(\frac{1}{2}\boldsymbol{S}^\top\boldsymbol{J}\boldsymbol{S}\right)^{\lambda_{12}} - \frac{\varsigma}{2}\tilde{\gamma}^2 \\
&+ \frac{\varsigma}{2}\gamma^2 + \frac{\bar{d}}{4\chi} + \frac{\Im}{2\chi}
\end{aligned}
$$

$$\leq -cV_1 + \vartheta_c \tag{31}$$

where $c = \min\{\kappa_{11}, \kappa_{12}, \sigma\varsigma\}$, $\lambda_{11} = \frac{1}{2}(\alpha_1 + 1) > 1$, $0 < \lambda_{12} = \frac{1}{2}(\beta_1 + 1) < 1$, $\kappa_{11} = 2^{\lambda_{11}} 3^{1-\lambda_{11}} \lambda_{\min}(\boldsymbol{K}_{11}) / \lambda_{\max}(\boldsymbol{J})$, $\kappa_{12} = 2^{\lambda_{12}} \lambda_{\min}(\boldsymbol{K}_{12}) / \lambda_{\max}(\boldsymbol{J})$, $\vartheta_c = \frac{\varsigma}{2}\gamma^2 + \frac{\bar{d}}{4\chi} + \frac{\Im}{2\chi} < \infty$ according to the boundedness of $\gamma, \chi, \bar{d}, \Im$ and $\bar{\Im}$. Based on the boundedness theorem, $\boldsymbol{S}$ and $\hat{\gamma}$ are uniformly ultimately bounded.

(ii) The feasibility of (8) and (9) can be verified by the following arguments. From (22) and (31), it is straightforward to prove that $\|\boldsymbol{S}\|$ is bounded. Since the second term $\|\text{sign}(q_{e0})\boldsymbol{f}(\boldsymbol{q}_{ev})\|$ in (16) is also bounded according to the definition of $\boldsymbol{f}(\boldsymbol{q}_{ev})$ and the fact that $|q_{ei}| \leq 1,\ i = 1, 2, 3$ as $\|\boldsymbol{q}_e\| = 1$. Then $\|(\boldsymbol{\omega} - \mu\hat{\boldsymbol{\omega}})V_r\|$ is bounded. If we assume that V_r is unbounded, then it follows that $\boldsymbol{\omega} = \mu\hat{\boldsymbol{\omega}}$. Then, one has

$$\dot{V}_p = \frac{\partial V_p}{\partial \boldsymbol{q}_e}\dot{\boldsymbol{q}}_e = \frac{1}{2}\nabla V_p^\top (\boldsymbol{q}_e \otimes \tilde{\boldsymbol{\omega}}) = -\text{Vec}(\boldsymbol{q}_e{}^* \otimes \nabla V_p)^\top \text{Vec}(\boldsymbol{q}_e{}^* \otimes \nabla V_p) \leq 0$$

which implies that V_p is bounded. Hence, V_r is bounded, which contradicts to the assumption. Therefore, V_r is bounded, which means (8) and (9) are satisfied.

(iii) To analyze the practical fixed-time stability, we construct a Lyapunov function as follows:

$$V_2 = \frac{1}{2}\boldsymbol{S}^\top \boldsymbol{J}\boldsymbol{S} \tag{32}$$

Considering system (3) and (4) with control law (18), the derivative of V_2 with respect to t can be given by

$$\begin{aligned}\dot{V}_2 =& \boldsymbol{S}^\top \boldsymbol{J}\dot{\boldsymbol{S}} + \frac{1}{2}\boldsymbol{S}^\top \dot{\boldsymbol{J}}\boldsymbol{S} \\ \leq& V_r \boldsymbol{S}^\top \Big(-\boldsymbol{K}_{21}\text{sig}^{\alpha_1}(\boldsymbol{S}) - \boldsymbol{K}_{22}\text{sig}^{\beta_1}(\boldsymbol{S}) \Big) \\ &+ \tilde{\gamma}\eth\|\boldsymbol{S}\|^2 + \frac{\bar{d}}{4\chi} + \frac{\Im}{2\chi}\end{aligned} \tag{33}$$

As is proved in property 1 and property 2, $\boldsymbol{S}$, $\hat{\gamma}$ and V_r are bounded. According to the definition of $\hat{\boldsymbol{\omega}}$ and ∇V_r, $\hat{\boldsymbol{\omega}}$ and ∇V_r are bounded since V_r is bounded. Then, in view of the definition of $\boldsymbol{S}$, $\boldsymbol{\omega}$ is bounded since V_r and $\hat{\boldsymbol{\omega}}$ are bounded. Then, $\dot{V}_r$, $\dot{\boldsymbol{f}}(\boldsymbol{q}_{ev})$ and $\dot{\hat{\boldsymbol{\omega}}}$ are bounded. Hence, there must exist a positive constant ϑ such that $\tilde{\gamma}\eth\|\boldsymbol{S}\|^2 + \frac{\bar{d}}{4\chi} + \frac{\Im}{2\chi} \leq \vartheta$. Therefore, according to Lemma 3 and

Lemma 4, we can obtain that

$$\begin{aligned}\dot{V}_2 &\leq \boldsymbol{S}^{\top}\left(-\boldsymbol{K}_{21}\mathrm{sig}^{\alpha_1}(\boldsymbol{S})-\boldsymbol{K}_{22}\mathrm{sig}^{\beta_1}(\boldsymbol{S})\right)+\vartheta \\ &\leq -\kappa_{11}{V_2}^{\lambda_{11}}-\kappa_{12}{V_2}^{\lambda_{12}}+\vartheta \end{aligned} \tag{34}$$

where $\kappa_{11},\ \kappa_{12},\ \lambda_{11},\ \lambda_{12}$ has been defined in (31). In view of Lemma 1, the trajectories of the closed-loop system (34) is bounded in fixed time T_1 as

$$\left\{\lim_{t\to T_1}\boldsymbol{S}(t)\mid V_2\leq \min\left\{\kappa_{11}^{-\frac{1}{\lambda_{11}}}\left(\frac{\vartheta}{1-\theta}\right)^{\frac{1}{\lambda_{11}}},\kappa_{12}^{-\frac{1}{\lambda_{12}}}\left(\frac{\vartheta}{1-\theta}\right)^{\frac{1}{\lambda_{12}}}\right\}\right\} \tag{35}$$

and the fixed-time T_1 is bounded by $T_1\leq 1/\left(\kappa_{11}\theta\left(\lambda_{11}-1\right)\right)+1/\left(\kappa_{12}\theta\left(1-\lambda_{12}\right)\right)$, θ is a scalar satisfying $0<\theta\leq 1$.

According to (35), it is straightforward to obtain that

$$\|\boldsymbol{S}\|\leq S_m=\sqrt{\min\left\{2\kappa_{11}^{-\frac{1}{\lambda_{11}}}\left(\frac{\vartheta}{1-\theta}\right)^{\frac{1}{\lambda_{11}}},2\kappa_{12}^{-\frac{1}{\lambda_{12}}}\left(\frac{\vartheta}{1-\theta}\right)^{\frac{1}{\lambda_{12}}}\right\}} \tag{36}$$

(iv) When $t>T_1$, one has $\|\boldsymbol{S}\|\leq S_m$. Then, to analyze the fixed-time stability, a Lyapunov function is constructed as follows:

$$V_3=\frac{1}{2}\left[\boldsymbol{q}_{ev}^{\top}\boldsymbol{q}_{ev}+\left(1-\mathrm{sign}\left(q_{e0}\right)q_{e0}\right)^2\right] \tag{37}$$

in which there are two equilibriums $(\boldsymbol{q}_I,\ -\boldsymbol{q}_I)$. Since V_r is bounded, then we can obtain $\|\hat{\boldsymbol{\omega}}\|<\varepsilon_{\hat{\omega}}$. Noting the fact that $\|\boldsymbol{q}_{ev}\|\leq 1$, and $V_r>\varrho$ according to Lemma 5, thus, the derivative of V_3 with respect to t is given by

$$\begin{aligned}\dot{V}_3 &= -\frac{1}{2V_r}\boldsymbol{q}_{ev}^{\top}\boldsymbol{f}(\boldsymbol{q}_{ev})+\mathrm{sign}\left(q_{e0}\right)\frac{\mu}{2}\boldsymbol{q}_{ev}^{\top}\hat{\boldsymbol{\omega}}+\mathrm{sign}\left(q_{e0}\right)\frac{1}{2V_r}\boldsymbol{q}_{ev}^{\top}\boldsymbol{S} \\ &\leq -\frac{1}{2V_r}\boldsymbol{q}_{ev}^{\top}\boldsymbol{f}(\boldsymbol{q}_{ev})+\vartheta_1 \end{aligned} \tag{38}$$

where $0<\vartheta_1\leq\frac{\mu}{2}\|\boldsymbol{q}_{ev}\|\|\hat{\boldsymbol{\omega}}\|+\|\boldsymbol{q}_{ev}\|\|\boldsymbol{S}\|/\left(2V_r\right)\leq\mu\varepsilon_{\hat{\omega}}/2+S_m/\left(2\varrho\right)<\infty$. Noting that the inequality $\left(1-|q_{e0}|\right)^2\leq\left(1-q_{e0}\right)\left(1+q_{e0}\right)=\boldsymbol{q}_{ev}^{\top}\boldsymbol{q}_{ev}$ holds, hence, we can obtain that $V_3\leq\boldsymbol{q}_{ev}^{\top}\boldsymbol{q}_{ev}$ from (37). Then, we consider the following two cases.

Case I: for the case of $|q_{ei}|\geq\varepsilon$, according to the definition of $\boldsymbol{f}(\boldsymbol{q}_{ev})$ in (17), Lemma 3 and Lemma 4, it follows that

$$\dot{V}_3\leq -\kappa_{21}{V_3}^{\lambda_{21}}-\kappa_{22}{V_3}^{\lambda_{22}}+\vartheta_1 \tag{39}$$

where $\lambda_{21} = \frac{1}{2}(\alpha_2+1) > 1$, $0 < \lambda_{22} = \frac{1}{2}(\beta_2+1) < 1$, $\kappa_{21} = \frac{k_{21}}{2V_{r,\max}} 3^{1-\lambda_{21}}$ and $\kappa_{22} = \frac{k_{22}}{2V_{r,\max}}$. From Lemma 2 , we can conclude that the trajectory of the closed-loop system is practical fixed-time stable and it will converge to a small neighborhood D_2 within T_2 after the system trajectory reaches the neighborhood of sliding surface satisfying $\|\boldsymbol{S}\| \le S_m$, where $T_2 \le 1/(\kappa_{22}\theta_1(1-\lambda_{22})) + 1/(\kappa_{21}\theta_1(\lambda_{21}-1))$,

$$D_2 : \left\{ \lim_{t\to T_3} V_3(\boldsymbol{q}_e(t)) \le \min\left\{ \kappa_{21}^{-\frac{1}{\lambda_{21}}} \left(\frac{\vartheta_1}{1-\theta_1}\right)^{\frac{1}{\lambda_{21}}}, \kappa_{22}^{-\frac{1}{\lambda_{22}}} \left(\frac{\vartheta_1}{1-\theta_1}\right)^{\frac{1}{\lambda_{22}}} \right\} \right\}$$

and θ_1 is a scalar satisfying $0 < \theta_1 \le 1$. This implies $\lim_{t\to T_3} \|\boldsymbol{q}_{ev}\| \le \varepsilon_{ev}$, with

$$\varepsilon_{ev} := \sqrt{\min\left\{ 2\kappa_{21}^{-\frac{1}{\lambda_{21}}} \left(\frac{\vartheta_1}{1-\theta_1}\right)^{\frac{1}{\lambda_{21}}}, 2\kappa_{22}^{-\frac{1}{\lambda_{22}}} \left(\frac{\vartheta_1}{1-\theta_1}\right)^{\frac{1}{\lambda_{22}}} \right\}} \tag{40}$$

where $T_3 = T_1 + T_2$.

Case II: If $|q_{ei}| < \varepsilon$, similar to Case I, one has

$$\dot{V}_3 \le -\theta_2\eta V_3 - (1-\theta_2)\eta V_3 + \vartheta_1 \tag{41}$$

where $\eta = \frac{l_1}{2V_{r,\max}}$, and $0 < \theta_2 \le 1$. Clearly, if $V_3 \ge \vartheta_1/(1-\theta_2)\eta$, then $\dot{V}_3 \le -\theta_2\eta V_3 \le 0$. Thus, all states in the closed-loop system (3) are bounded.

From the results (39) with $|q_{ei}| \ge \varepsilon$, it shows that the attitude tracking errors will converge to the region $|q_{ei}| \le \varepsilon_q$ in the fixed-time T_3, with $\varepsilon_q := \max\{\varepsilon_{ev}, \varepsilon\}$. Then, from definition of $\hat{\boldsymbol{\omega}}$ and $\boldsymbol{f}(\boldsymbol{q}_{ev})$, it yields that $\lim_{t\to T_3} \|\hat{\boldsymbol{\omega}}\| \le \varepsilon_{\hat{\omega}}$ and $\lim_{t\to T_3} |f_i(\boldsymbol{q}_{ev})| \le \varepsilon_f := k_{21}\varepsilon_q^{\alpha_2} + k_{22}\varepsilon_q^{\beta_2}$. Since V_r is bounded, then, observing the sliding mode surface $\boldsymbol{S}$ defined in (16), it follows that the velocity tracking errors converge to the region $|\omega_i| \le \varepsilon_\omega$ in the fixed-time T_3, with $\varepsilon_\omega := \mu\varepsilon_{\hat{\omega}} + (\varepsilon_f + S_m)/\varrho$. This completes the proof. □

To facilitate the implementation of the proposed control scheme, **Algorithm 1** is given below.

Remark 2. Since the quaternion is adopted, then each attitude corresponds to two different quaternions, i.e., $\boldsymbol{q}_I$ and $-\boldsymbol{q}_I$. In most of the existing literatures, only $\boldsymbol{q}_I$ is treated as a stable equilibrium and this is called the unwinding phenomenon (spacecraft rotates through an unnecessary large angle), which leads

Algorithm 1

1: Obtain V_p, V_r, ∇V_p, ∇V_r and $\nabla^2 V_p$ with parameters of attitude pointing constraints ϱ_{1j} and ϱ_2 and the desired attitude $\boldsymbol{q}_d$ according to (12), (13) and (14).

2: Obtain $\boldsymbol{S}$ with ∇V_p and $\boldsymbol{f}(\boldsymbol{q}_{ev})$ according to (16).

3: Obtain adaptive compensation part $\boldsymbol{u}_{ad}$ according to (19) and (3).

4: Obtain the controller $\boldsymbol{u}$ with $\boldsymbol{S}$, V_r, ∇V_r, $\nabla^2 V_p$ and $\boldsymbol{u}_{ad}$ according to (18).

5: Solve the dynamic equations (3),(4) with $\boldsymbol{u}$, (20) with the initial state $\boldsymbol{q}_e(0), \boldsymbol{\omega}(0)$ and $\hat{\gamma}(0)$.

to extra energy cost and longer maneuver time [29]. Here, it is avoided by introducing the term sign (q_{e0}) to the sliding surface $\boldsymbol{S}$ and potential function.

Remark 3. To implement the proposed control scheme, it is necessary to select appropriate parameters for controller. Then, the tuning ideas are given as follows. According to the formulation of T_1, the smaller the convergence time of sliding mode is, the smaller the controller parameter α_1 and the bigger the controller parameters $\boldsymbol{K}_{11}$, $\boldsymbol{K}_{12}$ and β_1 are required, which causes more control effort. With the definition of T_2, it follows that the controller parameters k_{21}, k_{22}, α_2 and β_2 determine the convergence time of the attitude error, the smaller the convergence time of attitude tracking error, the smaller the controller parameter α_1 and the bigger the controller parameters k_{21}, k_{22} and β_2 are required, but yield more energy consumption.

4. Numerical example

Assume that the photosensitive sensor and the high-gain communication antenna are located on the y axis and the z axis of the spacecraft's body frame, respectively. Noting that both of the initial and the desired attitude must be outside the forbidden zones and inside mandatory zone.

To manifest the fixed-time stability, anti-unwinding performance and the uncertainty rejection capability of the proposed controller. Two numerical ex-

amples are given to demonstrate the effectiveness of the proposed method. The first one is used to verify the fixed-time convergence and the uncertainty rejection capability of the proposed control algorithm. To verify the anti-unwinding performance, the second one is conducted with different initial attitude error quaternion from the first one, such as $q_{e0} > 0$ or $q_{e0} < 0$. The norm inertia matrix of spacecraft $\boldsymbol{J}_0$ is set as $\mathrm{diag}(10, 12, 14)$, for the rest-to-rest problem, both of the initial and desired angular velocity are set as $\boldsymbol{\omega}(0) = [0, 0, 0]^\top$, $\boldsymbol{\omega}_d = [0, 0, 0]^\top$. The uncertainties of disturbance torque and inertia matrix of spacecraft are considered, which are set as

$$\boldsymbol{d} = 0.02\left[\sin(0.4t) + 1, \cos(0.4t) + 1, \sin(0.4t) + 1\right]^\top \tag{42}$$

$$\Delta\boldsymbol{J} = 0.02\begin{bmatrix} \sin(0.4t) & \cos(0.4t) & \sin(0.4t) \\ \cos(0.4t) & \cos(0.4t) & \cos(0.4t) \\ \sin(0.4t) & \cos(0.4t) & \sin(0.4t) \end{bmatrix} \tag{43}$$

Moreover, the measurement noise of angular velocity is considered, which is formulated as $\boldsymbol{\omega}_m = \boldsymbol{\omega} + \boldsymbol{\delta}$, where $\boldsymbol{\omega}_m$ is the measurement output of angular velocity and $\boldsymbol{\delta} = 10^{-4}\left[\sin(5t), \cos(5t), -\sin(5t)\right]^\top$.

4.1. Example 1

In the first example, the initial and desired attitude are set as $\boldsymbol{q}(0) = [0.8074, 0.5390, 0.2000, 0.1326]^\top$, $\boldsymbol{q}_d = [0.8150, -0.1000, -0.3500, 0.4509]^\top$ respectively, which means $q_{e0}(0) > 0$. The parameters of the attitude forbidden zones and the attitude mandatory zone are listed in Table 1. The parameters of the controller Eq.(58) in [2] are listed in a table 2.

The trajectories of attitude error quaternion, angular velocity and control inputs are plotted in Fig. 2, Fig. 3 and Fig. 4 respectively. Under the uncertainties of inertia matrix and external disturbances and small measurement noise, the attitude trajectories of the proposed controller converge to the desired attitude at almost $19s$, simultaneously, the steady accuracy of attitude error and angular velocity error are less than $3 * 10^{-4}$. In addition, the convergence speed and steady-state accuracy with the proposed control scheme are better than

controller in [2]. As discussed above, fixed-time convergence and uncertainty rejection capability of the proposed controller are verified.

Table 1: Parameters of attitude constraints (8) and (9).

Mandatory Zone	$\boldsymbol{x}_2 = [-0.2676, -0.8236, 0.5001]^\top$,	θ_{2max}=60 deg
Forbidden Zone	$\boldsymbol{x}_{11} = [-0.8926, 0.4375, 0.1091]^\top$,	θ_{1min}=15 deg
Forbidden Zone	$\boldsymbol{x}_{12} = [0.2939, 0.9045, -0.3090]^\top$,	θ_{2min}=40 deg
Forbidden Zone	$\boldsymbol{x}_{13} = [-0.0812, 0.7442, 0.6630]^\top$,	θ_{3min}=20 deg

The obtained 3D and 2D attitude trajectories of $\boldsymbol{y}_1^{'}$ and $\boldsymbol{y}_2^{'}$ are plotted in Fig. 4 and Fig. 5, respectively. The "circle" and "star" denote initial and the desired position of $\boldsymbol{y}_1^{'}$ and $\boldsymbol{y}_2^{'}$, respectively. As shown in these figures, the attitude trajectories generated by proposed controller and controller Eq.(58) in [2] both arrive at the desired attitude quaternion $\boldsymbol{q}_d$. In addition, the satisfaction of attitude pointing constraints (8) and (9) can also be verified, since the trajectory of $\boldsymbol{y}_2^{'}$ stay in the mandatory zones and the trajectory of $\boldsymbol{y}_1^{'}$ do not touch the forbidden zones during the attitude maneuver. Compared with controller Eq.(58) in [2], the length of trajectory $\boldsymbol{y}_1^{'}$ and $\boldsymbol{y}_2^{'}$ under proposed controller is shorter.

4.2. Example 2

In this example, the initial and desired attitude are set as $\boldsymbol{q}(0) = [0.8174, 0.5390, 0.2000, 0.0366]^\top$, $\boldsymbol{q}_d = [-0.5900, 0.1000, 0.3500, -0.7207]^\top$, which means that

Table 2: Parameters of controllers.

The controller in [2] Eq.(58)	$\alpha = 30$, $k_{11} = k_{12} = k_{13} = k_2 = 1.5$
The proposed controller	$\alpha_1 = \alpha_2 = 0.8$, $\varrho_{11} = \varrho_{12} = \varrho_{13} = \varrho_2 = 1.5$,
	$\beta_1 = \beta_2 = 3$, $\sigma = 0.013$, $\varsigma = 0.01$, $\delta = 100$
	$k_{11} = k_{12} = k_{22} = 1$, $k_{21} = 4$
	$\hat{J}_n(0) = 0.01$, $\mu = 0.01$.

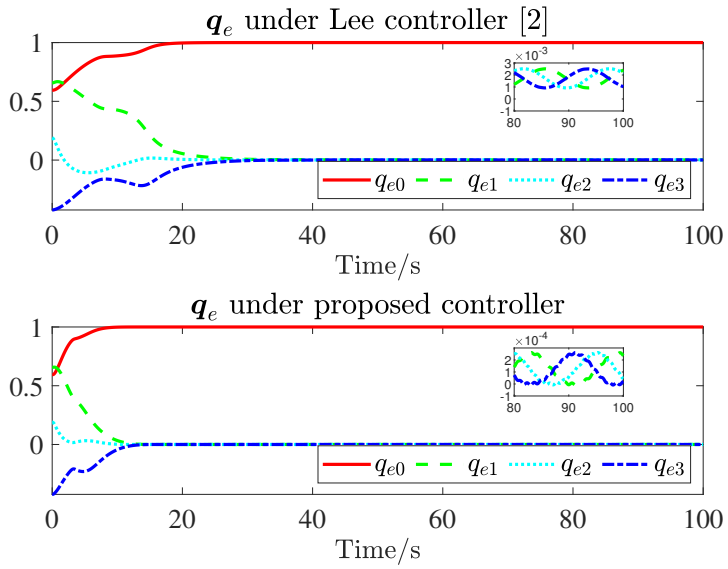

Fig. 2. The scalar of attitude error quaternion q_{e0}.

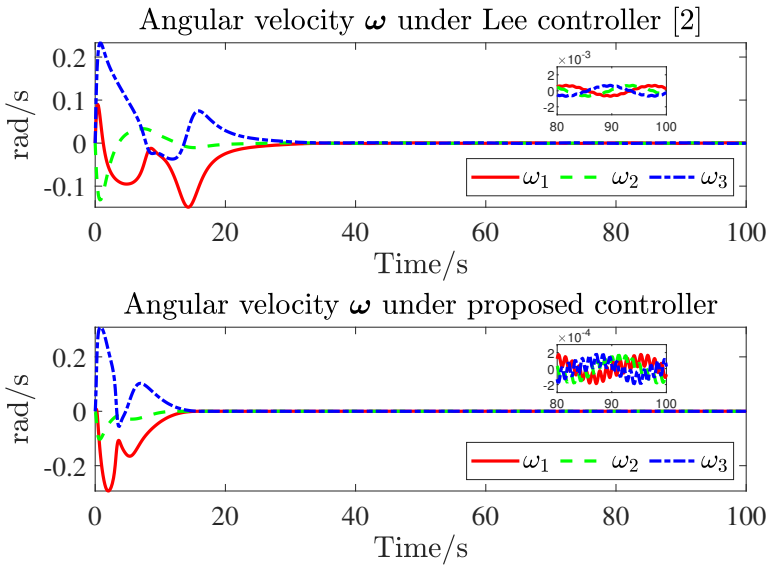

Fig. 3. Angular velocity.

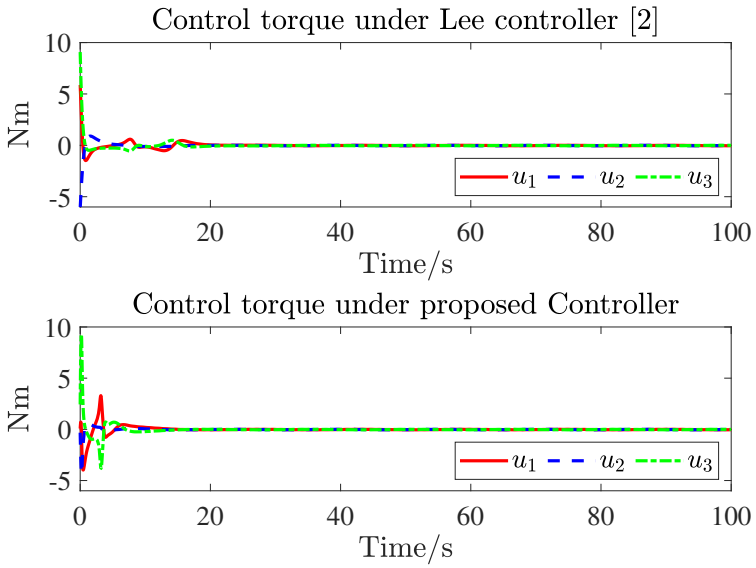

Fig. 4. Control torque.

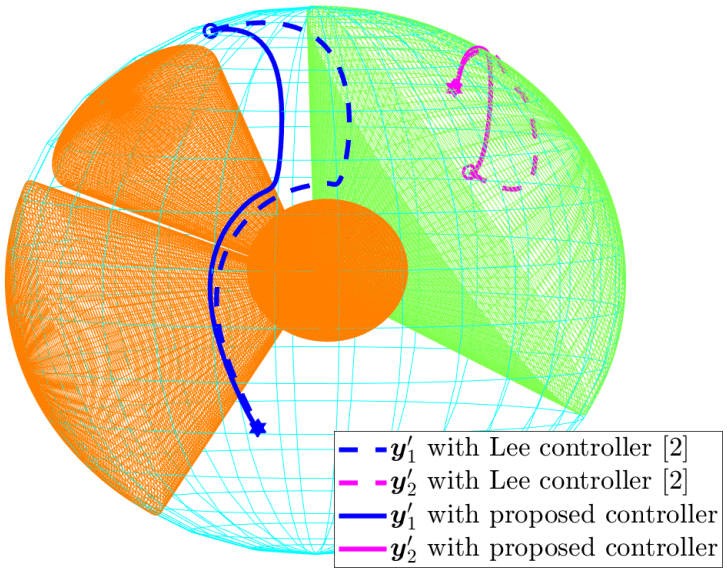

Fig. 5. 3D trajectories.

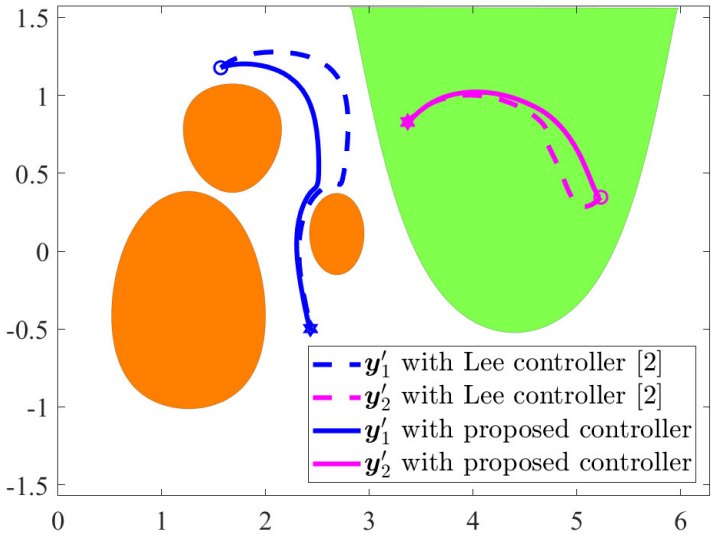

Fig. 6. 2D trajectories.

$q_{e0}(0) < 0$. The parameters of the attitude forbidden zones and the attitude mandatory zone are listed in Table 1, and the proposed controller parameters are listed in a table 3.

Compared with example 1, for the case of $q_{e0}(0) > 0$, the attitude error quaternion converge to the equilibrium point $\boldsymbol{q}_I$, and for the case of $q_{e0}(0) < 0$, the attitude error quaternion converge to the equilibrium point $-\boldsymbol{q}_I$, which verifies the anti-unwingding performance of the proposed controller and controller in [2].

Table 3: Parameters of controllers.

The controller in [2] Eq.(58)	$\alpha = 40$, $k_{11} = k_{12} = k_{13} = k_2 = 1.2$
The proposed controller	$\alpha_1 = \alpha_2 = 0.8$, $\varrho_{11} = \varrho_{12} = \varrho_{13} = \varrho_2 = 1.5$,
	$\beta_1 = \beta_2 = 3$, $\sigma = 0.02$, $\varsigma = 0.01$, $\delta = 100$
	$k_{11} = k_{12} = k_{22} = 1$, $k_{21} = 2.5$
	$\hat{J}_n(0) = 0.01$, $\mu = 0.01$.

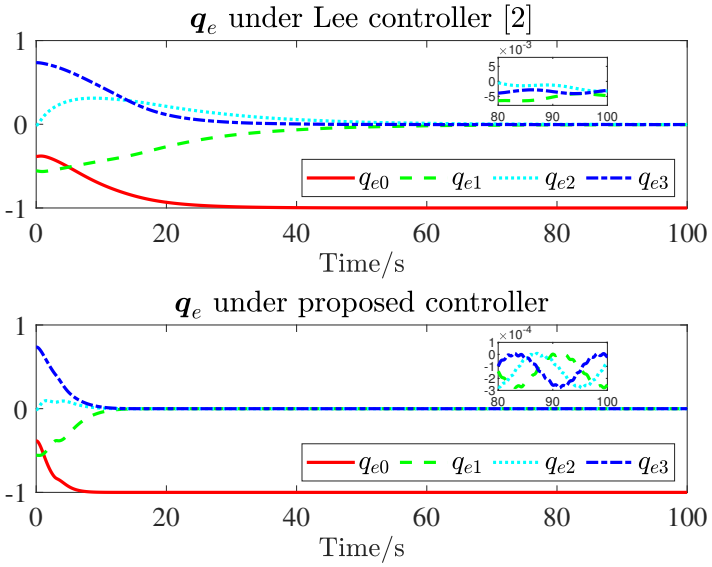

Fig. 7. The scalar of attitude error quaternion q_{e0}.

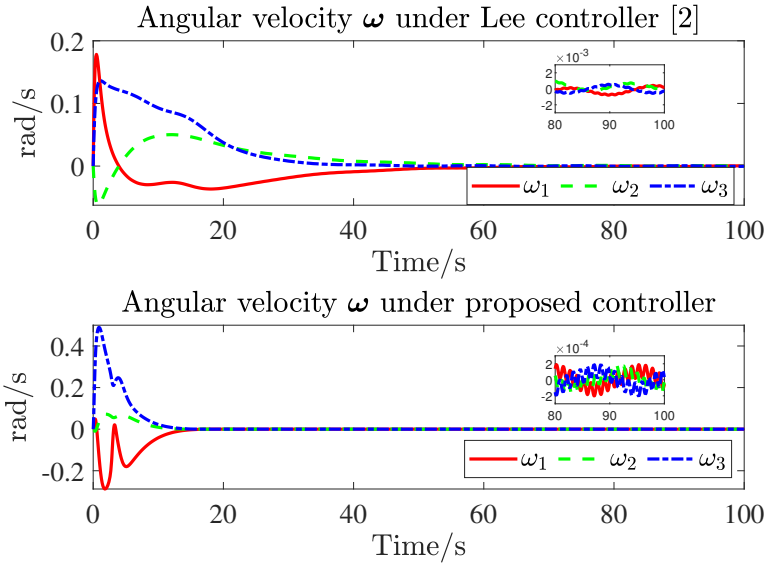

Fig. 8. Angular velocity.

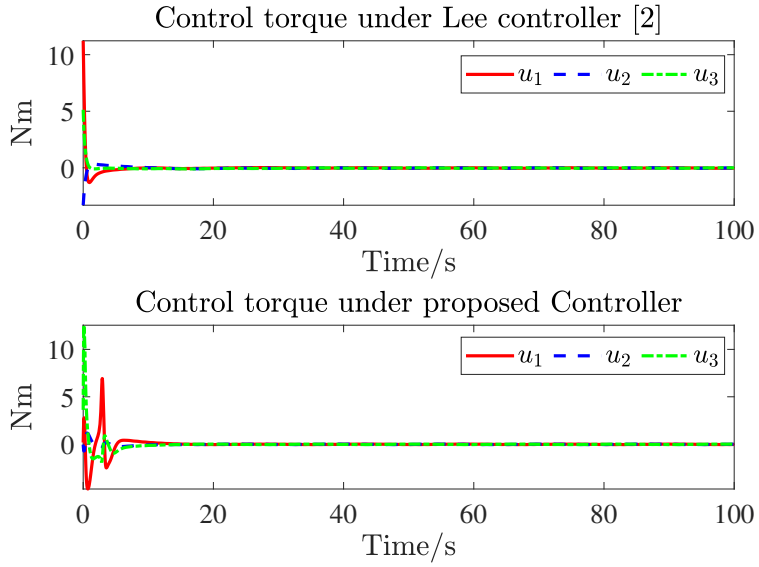

Fig. 9. Control torque.

The obtained 3D and 2D attitude trajectories of $\boldsymbol{y}_1^{'}$ and $\boldsymbol{y}_2^{'}$ are plotted in Fig. 10 and Fig. 11, respectively. As shown in these figures, the satisfaction of attitude pointing constraints (8) and (9) can also be verified, in the presence of disturbance uncertainty, the trajectory of $\boldsymbol{y}_2^{'}$ stay in the mandatory zones and the trajectory of $\boldsymbol{y}_1^{'}$ do not touch the forbidden zones during the attitude maneuver.

5. Conclusion

In this paper, a novel attitude controller is designed to maintain the fixed-time convergence and the satisfaction of attitude pointing constraints while considering the inertial uncertainty and external disturbance torque for spacecraft reorientation maneuvers. A novel PF-based non-singular fixed-time anti-unwinding sliding surface is constructed, which not only inherits the advantages of non-singular fixed-time SMC, but also has the ability to address the attitude pointing constraints. The unwinding phenomenon raised by quaternion

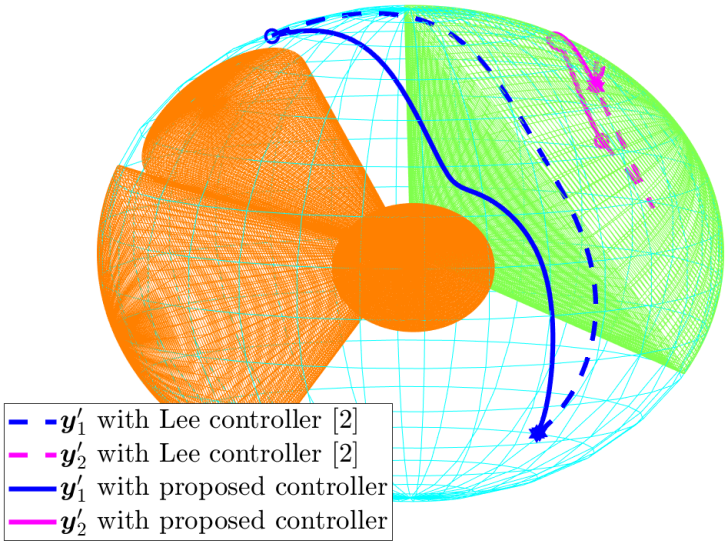

Fig. 10. 3D trajectories.

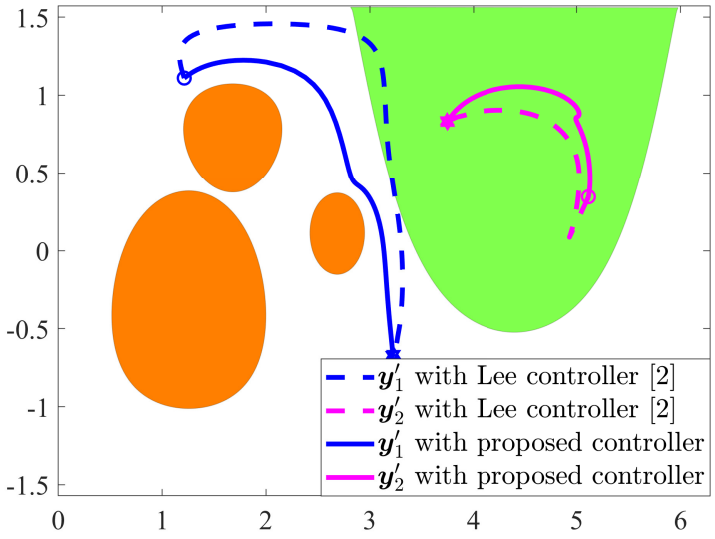

Fig. 11. 2D trajectories.

redundancy is avoided with the designed sliding manifold and potential function. Moreover, by introducing adaptive parameters to estimate system lumped disturbance, the capability of disturbance rejection can be guaranteed with the proposed adaptive SMC scheme and update strategy of parameters, meanwhile, the fixed-time stability has been proven by employing rigorous Lyapunov analyses.

Declaration of competing interest

The authors declare that they have no known competing financial interests or personal relationships that could have appeared to influence the work reported in this paper.

References

[1] B. Jiang, Q. Hu, M. I. Friswell, Fixed-time attitude control for rigid spacecraft with actuator saturation and faults, IEEE Trans Control Syst Technol 24 (2016) 1892–1898. doi:10.1109/TCST.2016.2519838.

[2] U. Lee, M. Mesbahi, Feedback control for spacecraft reorientation under attitude constraints via convex potentials, IEEE Trans Aerosp Electron Syst 50 (2014) 2578–2592. doi:https://doi.org/10.1109/TAES.2014.120240.

[3] H. C. Kjellberg, E. G. Lightsey, Discretized constrained attitude pathfinding and control for satellites, J Guid Control Dyn 36 (2013) 1301–1309. doi:https://doi.org/10.2514/1.60189.

[4] S. Tanygin, Fast three-axis constrained attitude pathfinding and visualization using minimum distortion parameterizations, J Guid Control Dyn 38 (2015) 2324–2336. doi:https://doi.org/10.2514/1.G000974.

[5] V. I. Utkin, Scope of the Theory of Sliding Modes, Springer Berlin Heidelberg, 1992.

[6] C. Edwards, S. Spurgeon, Sliding mode control: theory and applications, Crc Press, 1998.

[7] E. M. Jafarov, Variable structure control and time-delay systems, A Series of Reference Books and Textbooks, Europe Office (2009).

[8] Y. Shtessel, C. Edwards, L. Fridman, A. Levant, et al., Sliding mode control and observation, volume 10, Springer, 2014.

[9] B. Draženović, The invariance conditions in variable structure systems, Automatica 5 (1969) 287–295.

[10] V. Utkin, J. Guldner, J. Shi, Sliding mode control in electro-mechanical systems, CRC press, 2017.

[11] A. Sofyalı, E. M. Jafarov, Robust stabilization of spacecraft attitude motion under magnetic control through time-varying integral sliding mode, International Journal of Robust and Nonlinear Control 29 (2019) 3446–3468.

[12] A. Sofyalı, E. M. Jafarov, R. Wisniewski, Robust and global attitude stabilization of magnetically actuated spacecraft through sliding mode, Aerospace Science and Technology 76 (2018) 91–104.

[13] E. Abdulhamitbilal, E. M. Jafarov, Sliding mode attitude controller design for nonlinear flexible geosynchronous satellite with thrust jets, in: 2008 International Workshop on Variable Structure Systems, IEEE, 2008, pp. 221–226.

[14] H. Du, S. Li, C. Qian, Finite-time attitude tracking control of spacecraft with application to attitude synchronization, IEEE Trans. Autom. Control 56 (2011) 2711–2717. doi:https://doi.org/10.1109/TAC.2011.2159419.

[15] Q. Hu, X. Tan, M. R. Akella, Finite-time fault-tolerant spacecraft attitude control with torque saturation, J Guid Control Dyn 40 (2017) 2524–2537. doi:https://doi.org/10.2514/1.G002191.

[16] R. Dong, A. Wu, Y. Zhang, G.-R. Duan, Anti-unwinding sliding mode attitude control via two modified rodrigues parameter sets for spacecraft, Automatica 129 (2021) 109642. doi:https://doi.org/10.1016/j.automatica.2021.109642.

[17] K. Lu, Y. Xia, Adaptive attitude tracking control for rigid spacecraft with finite-time convergence, Automatica 49 (2013) 3591–3599. doi:https://doi.org/10.1016/j.automatica.2013.09.001.

[18] X. Yu, M. Zhihong, Fast terminal sliding-mode control design for nonlinear dynamical systems, IEEE Transactions on Circuits and Systems I: Fundamental Theory and Applications 49 (2002) 261–264. doi:https://doi.org/10.1109/81.983876.

[19] S. Yu, X. Yu, B. Shirinzadeh, Z. Man, Continuous finite-time control for robotic manipulators with terminal sliding mode, Automatica 41 (2005) 1957–1964. doi:https://doi.org/10.1016/j.automatica.2005.07.001.

[20] A. Polyakov, Nonlinear feedback design for fixed-time stabilization of linear control systems, IEEE Trans. Autom. Control 57 (2012) 2106–2110. doi:https://doi.org/10.1109/TAC.2011.2179869.

[21] X. Shi, Z. Zhou, D. Zhou, Finite-time attitude trajectory tracking control of rigid spacecraft, IEEE Trans Aerosp Electron Syst 53 (2017) 2913–2923. doi:https://doi.org/10.1109/TAES.2017.2720298.

[22] Z. Song, H. Li, K. Sun, Finite-time control for nonlinear spacecraft attitude based on terminal sliding mode technique, ISA Trans 53 (2014) 117–124. doi:https://doi.org/10.1016/j.isatra.2013.08.008.

[23] A. Zou, K. D. Kumar, A. H. de Ruiter, Fixed-time attitude tracking control for rigid spacecraft, Automatica 113 (2020) 108792. doi:https://doi.org/10.1016/j.automatica.2019.108792.

[24] L. Cao, B. Xiao, M. Golestani, Robust fixed-time attitude stabilization control of flexible spacecraft with actuator uncertainty, Nonlinear Dynamics 100 (2020) 2505–2519.

[25] R. Xu, H. Wang, W. Xu, P. Cui, S. Zhu, Rotational-path decomposition based recursive planning for spacecraft attitude reorientation, Acta Astronaut. 143 (2018) 212–220. doi:https://doi.org/10.1016/j.actaastro.2017.11.035.

[26] D. Y. Lee, R. Gupta, U. V. Kalabić, S. Di Cairano, A. M. Bloch, J. W. Cutler, I. V. Kolmanovsky, Geometric mechanics based nonlinear model predictive spacecraft attitude control with reaction wheels, J Guid Control Dyn 40 (2017) 309–319. doi:https://doi.org/10.2514/1.G001923.

[27] R. G. Melton, Hybrid methods for determining time-optimal, constrained spacecraft reorientation maneuvers, Acta Astronaut. 94 (2014) 294–301. doi:https://doi.org/10.1016/j.actaastro.2013.05.007.

[28] Y. Geng, C. Li, Y. Guo, J. D. Biggs, Fixed-time near-optimal control for repointing maneuvers of a spacecraft with nonlinear terminal constraints, ISA Trans 97 (2020) 401–414. doi:10.1016/j.isatra.2019.07.026.

[29] Q. Hu, B. Chi, M. R. Akella, Anti-unwinding attitude control of spacecraft with forbidden pointing constraints, J Guid Control Dyn 42 (2019) 822–835. doi:https://doi.org/10.2514/1.G003606.

[30] Q. Shen, C. Yue, C. H. Goh, B. Wu, D. Wang, Rigid-body attitude stabilization with attitude and angular rate constraints, Automatica 90 (2018) 157–163. doi:https://doi.org/10.1016/j.automatica.2017.12.029.

[31] J. Yang, Y. Duan, M. K. Ben-Larbi, E. Stoll, Potential field-based sliding surface design and its application in spacecraft constrained reorientation, J Guid Control Dyn 44 (2021) 399–409. doi:https://doi.org/10.2514/1.G005026.

[32] R.-Q. Dong, A.-G. Wu, Y. Zhang, Anti-unwinding sliding mode attitude maneuver control for rigid spacecraft, IEEE Transactions on Automatic Control 67 (2021) 978–985.

[33] Y. Guo, S.-M. Song, X.-H. Li, Quaternion-based finite-time control for attitude tracking of the spacecraft without unwinding, Int J Control Autom Syst 13 (2015) 1351–1359. doi:https://doi.org/10.1007/s12555-014-0318-7.

[34] M. H. Shahna, M. Abedi, An anti-unwinding finite time fault tolerant sliding mode control of a satellite based on accurate estimation of inertia moments, ISA Trans 101 (2020) 23–41. doi:https://doi.org/10.1016/j.isatra.

[35] Q. Hu, W. Chen, L. Guo, J. D. Biggs, Adaptive fixed-time attitude tracking control of spacecraft with uncertainty-rejection capability, IEEE Trans. Syst. Man Cybern. Syst. (2021) 1–14. doi:https://doi.org/10.1109/TSMC.2021.3100903.

[36] B. Huang, A.-j. Li, Y. Guo, C.-q. Wang, Fixed-time attitude tracking control for spacecraft without unwinding, Acta Astronautica 151 (2018) 818–827.

[37] M. N. Soorki, M. S. Tavazoei, Adaptive robust control of fractional-order swarm systems in the presence of model uncertainties and external disturbances, IET Control Theory & Applications 12 (2018) 961–969. doi:https://doi.org/10.1049/iet-cta.2017.0035.

[38] M. N. Soorki, T. V. Moghaddam, A. Emamifard, A new fast finite time fractional order adaptive sliding-mode control for a quadrotor, in: 2021 7th International Conference on Control, Instrumentation and Automation (ICCIA), 2021, pp. 1–5. doi:10.1109/ICCIA52082.2021.9403563.

[39] A. Astolfi, D. Karagiannis, R. Ortega, Nonlinear and adaptive control with

applications, volume 187, Springer, 2008. doi:https://doi.org/10.1007/978-1-84800-066-7.

[40] G. H. Hardy, J. E. Littlewood, G. Pólya, G. Pólya, et al., Inequalities, Cambridge university press, 1952. doi:https://doi.org/10.1017/S0025557200027455.

[41] A.-M. Zou, A. H. de Ruiter, K. D. Kumar, Distributed finite-time velocity-free attitude coordination control for spacecraft formations, Automatica 67 (2016) 46–53. doi:https://doi.org/10.1016/j.automatica.2015.12.029.

[42] B. Li, Y. Wang, K. Zhang, G.-R. Duan, Constrained feedback control for spacecraft reorientation with an optimal gain, IEEE Trans Aerosp Electron Syst 57 (2021) 3916–3926. doi:https://doi.org/10.1109/TAES.2021.3082696.